Science Advances
AAAS

Supplementary Materials for

Integration of feeding behavior by the liver circadian clock reveals network dependency of metabolic rhythms

Carolina M. Greco*, Kevin B. Koronowski, Jacob G. Smith, Jiejun Shi, Paolo Kunderfranco, Roberta Carriero, Siwei Chen, Muntaha Samad, Patrick-Simon Welz, Valentina M. Zinna, Thomas Mortimer, Sung Kook Chun, Kohei Shimaji, Tomoki Sato, Paul Petrus, Arun Kumar, Mireia Vaca-Dempere, Oleg Deryagian, Cassandra Van, José Manuel Monroy Kuhn, Dominik Lutter, Marcus M. Seldin, Selma Masri, Wei Li, Pierre Baldi, Kenneth A. Dyar, Pura Muñoz-Cánoves, Salvador Aznar Benitah*, Paolo Sassone-Corsi

*Corresponding author. Email: salvador.aznar-benitah@irbbarcelona.org (S.A.B.); grecoc@uci.edu (C.M.G.)

Published 22 September 2021, *Sci. Adv.* **7**, eabi7828 (2021)
DOI: 10.1126/sciadv.abi7828

The PDF file includes:

Other Supplementary Material for this manuscript includes the following:

Supplementary Materials and Methods

Next-Generation Sequencing Sample Preparation and Analysis

RNA-Sequencing

Following procedures previously described [13], total RNA was monitored for quality control using the Agilent Bioanalyzer Nano RNA chip and Nanodrop absorbance ratios for 260/280nm and 260/230nm for liver samples from WT, KO, Liver-RE AL and NF. Library construction was performed according to the Illumina TruSeq Total RNA stranded protocol (three biological replicates for all ZT points with the exception of ZT8 L-RE NF that has two biological replicates). The input quantity for total RNA was 1 μg, and rRNA was depleted using ribo-zero rRNA gold removal kit (human/mouse/rat). The rRNA-depleted RNA was chemically fragmented for 3 min. First-strand synthesis used random primers and reverse transcriptase to make cDNA. After second-strand synthesis, the ds cDNA was cleaned using AMPure XP beads and the cDNA was end repaired, and then the 3′ ends were adenylated. Partial stub oligos for Illumina adapters were ligated on the ends and the adapter ligated fragments were enriched and barcoded by nine cycles of PCR using unique dual indexing primers. The resulting libraries were validated by qPCR and sized by Agilent Bioanalyzer DNA high-sensitivity chip. The concentrations for the libraries were normalized and then multiplexed together. The pooled library concentration for denaturation was 2 nM, and the final concentration for loading was 400 pM. The multiplexed libraries were sequenced on the S2 flowcell using paired-end 100 cycles chemistry for the Illumina NovaSeq 6000. The version of NovaSeq control software was NVCS 1.6.0 with real-

time analysis software, RTA 3.4.4. Post-processing of the run to generate the FASTQ files was performed at the Institute for Genomics and Bioinformatics (UCI IGB). The paired-end reads from each replicate were separately aligned to the reference genome assembly mm10 and corresponding transcriptome using the Tuxedo protocol (Illumina) [86]. Reads uniquely aligned to known exons or splice junctions extracted with no more than two mismatches were included in the transcriptome. Reads uniquely aligned but with more than two mismatches, or reads matching several locations in the reference genome, were removed.

For time series datasets, rhythmic transcripts were detected with the non-parametric JTK_CYCLE algorithm [28] incorporating a period of 24 h. Genes were considered rhythmic over the circadian cycle if their permutation-based, adjusted *P*-value was < 0.01. Metabolites were evaluated with an adjusted *P*-value of < 0.05 given the inherent variability of metabolite quantification across mice and the *n*-value of this experiment. Additional detection of rhythmicity for transcripts was conducted using a different, independently generated algorithm – BIO_CYCLE [29]. Differential Rhythmicity analysis was carried out using LimoRhyde [30]. Starting rhythmicity detection was JTK_CYCLE; P <0.01. Transcripts were considered differentially rhythmic at pDR <0.01.

GO biological process (DIRECT) enrichment analysis was conducted using the Database for Annotation, Visualization and Integrated Discovery (DAVID) version 6.8 [87]. Transcription factors binding sites were analyzed in the promoter regions (−10000~

+2000 bps of TSS) of circadian genes. Binding sites were determined from experimental ChIP-Seq data and MotifMap [32] results for the mouse genome build mm10 (BBLS > 1, FDR < 0.25). A Fisher's exact test was performed between the circadian genes and the whole genome to establish enrichment.

For RNA-sequencing of AML12 cells and primary hepatocytes, library preparation and sequencing was performed by Novogene following standard procedures. Libraries were prepared using the NEBNext Ultra II RNA Library Prep (Illumina). Libraries were ran on a NovaSeq 6000. Raw paired (150x150) end reads were first quality checked with FastQC v0.11.8 and aligned to the to the reference genome assembly mm10 with the following settings (STAR--outFilterMultimapNmax 20 --alignSJoverhangMin 8 –alignSJDBoverhangMin 1 --outFilterMismatchNmax 999 --outFilterMismatchNoverReadLmax 0.04 --alignIntronMin 20--alignIntronMax 1000000 --alignMatesGapMax 1000000 --outSAMattributes NH HI NM MD). RNA-seq quality assessment was performed using RSeQC v3.0.1 tool [88]. Differential expression analysis was assessed with edgeR v3.30.0 R Bioconductor package [89] and only genes with a cut-off expression > 1 CPM in at least two samples were included in the analysis. TMM method was applied to normalize gene counts and glmQLFTest and decideTestsDGE functions were used to perform differential analysis, with a minimum cut-off of absolute fold change ≥ 1.2 and FDR ≤0.05. Complete list of differentially expressed genes and statistical information (pValue and FDR) for each condition are available at Gene Expression Omnibus (GEO: awaiting reference code).

Exon-Intron Analysis

For intron–exon analysis, reads were mapped to the mouse genome (mm9) using STAR v2.6.0c [90] with the option '--quantMode TranscriptomeSAM', and then gene expression level in FPKM was quantified using RSEM v1.3.1 [91]. The gene annotation file was downloaded from GENCODE (https://www.gencodegenes.org/mouse/release_M1.html), and the coordinates of exons and introns were generated from it. To avoid assigning the exon-junction reads to introns [92], introns were shrank by 10-bp at both 5′ and 3′ ends. The 'coverageBed' module in bedtools v2.25.0[93] was used to generate reads count in each intron/exon. The option of '-F 0.5' was used to make sure a particular read was not counted in both exon and intron. The reads count per kilobase per million reads (RPKM) was calculated as the expression level of each intron/exon normalized by both intron/exon length and the total intronic/exonic reads count of each sample. As the exonic-to-intronic ratio varies from sample to sample, exons and introns were processed separately.

Cross-Tissue Gene Correlation

All datasets, analysis and walk-through are provided at: https://github.com/marcus-seldin/endocrine_communication-nonrestored-clocks. Briefly, genes identified as network-dependent (this study) were taken from liver gene expression in the hybrid mouse diversity panel [94,95]. All peripheral genes (adipose, muscle, hypothalamus and intestine) from the same mice were then correlated across the network-dependent genes in liver, where the global levels of cross-tissue correlation were quantified as a Ssec score [49]. The Ssec score for each peripheral gene

was normalized to the average correlation for each given tissue, and scaled according to fold-change relative to the same Ssec for non-circadian genes. Collectively, this enabled us to pinpoint peripheral genes that correlated specifically with network-dependent liver genes. Pathway enrichment for muscle genes ranked by Ssec score was calculated and visualized using WebGestalt [96].

ChIP-Sequencing

Library construction was performed from two biological replicates using the NEBNext® Ultra DNA Library Prep for Illumina® kit (E7370) according to the manufacturer's protocol. Briefly, input and ChIP enriched DNA were subjected to end repair and addition of "A" bases to 3′ ends, ligation of adapters and USER excision. All purification steps were performed using AgenCourt AMPure XP beads (Beckman Coulter, A63882). Library amplification was performed by PCR using NEBNext® Multiplex Oligos for Illumina (Index Primers Set 1, ref. E7335), (Index Primers Set 2, ref. E7500), (Index Primers Set 3, ref. E7710) and (Index Primers Set 4, ref. E7730). Final libraries were analyzed using Agilent Bioanalyzer or Fragment analyzer High Sensitivity assay (ref. 5067-4626 or ref. DNF-474) to estimate the quantity and check size distribution, and were then quantified by qPCR using the KAPA Library Quantification Kit (ref. KK4835, KapaBiosystems) prior to amplification with Illumina's cBot. Libraries were sequenced 1 * 50+8 bp on Illumina's HiSeq2500. To profile CEBPB enriched regions, raw single end reads were first quality checked with FastQC v0.11.8 and aligned to the UCSC Mus Musculus release mm9, available at https://hgdownload.soe.ucsc.edu/goldenPath/mm9/bigZips/ using Bowtie2 v2.4.2 [97]

with the following settings (bowtie2 -q –local). Mapped reads were then sorted using Samtools [98] 1.9 and filtered with Sambamba v0.7.1 [99] with the following settings (sambamba view -h -t 2 -f bam -F "[XS] == null and not unmapped and not duplicate"). ChIP-seq quality assessment was performed using ChIPQC v1.26.0 R Bioconductor package [100]. CEBPB enriched regions relative to input DNA were assessed using the ENCODE recommended Irreproducibility Discovery Rate (IDR) framework. Peaks in both replicates were detected with MACS2 v2.2.7.1 [101] with the following settings (macs2 callpeak -f BAM -g 1.87e9 -B -p 1e-3). Peak consistency between true replicates were detected with IDR v2.0.4.2 (https://projecteuclid.org/journals/annals-of-applied-statistics/volume-5/issue-3/Measuring-reproducibility-of-high-throughput/10.1214/11-AOAS466.full) with the following settings (--input-file-type narrowPeak --rank p.value). Complete list of Peaks coordinates and statistical information (pValue and FDR) in each sample and between replicates are available at Gene Expression Omnibus (GEO: awaiting reference number). To compute the overlap between CEBPB enriched regions and previously published BMAL1 enriched regions [13], BMAL1 raw reads were retrieved from GEO:GSE132659 and were mapped, filtered, and peaks detected using the IDR framework. We then intersect CEBPB and BMAL1 peaks coordinates with Bedtools v2.30.0 with the following settings (bedtools intersect -b -a -u). Peak Annotation was assessed with ChIPseeker v1.26.0 R Bioconductor package [102] using the pre-build annotation database TxDb.Mmusculus.UCSC.mm9.knownGene (tssRegion=c(-2000, 2000)). Coverage tracks for each sample was computed with Bedtools bamCoverage option, with the following settings (bamCoverage --binSize 20 --normalizeUsing BPM

--smoothLength 60--extendReads 150 –centerReads). To obtain a global evaluation of enrichment around the transcription starting site (TSS), we used both the computeMatrix and plotHeatmap option of Bedtools package, with the following settings (computeMatrix reference-point --referencePoint TSS --beforeRegionStartLength 2000--afterRegionStartLength 2000 –skipZeros). Differential enrichment analysis was assessed with DiffBind v3.0.3 R Bioconductor package [103] using default system settings, providing pre-build DBA_BLACKLIST_MM9 black list coordinates and exporting reads with the following settings (bUsePval = TRUE,th = 0.05). Statistical analysis and visualization of functional profiles for genes and gene clusters associated with TSS region were computed with clusterProfiler R Bioconductor package v3.16.1 [104], using org.Mm.eg.db R Bioconductor annotation database, with a minimum threshold of FDR ≤0.05.

ATAC-Sequencing

The Omni-ATAC protocol for isolation of nuclei and library preparation [105] was followed. Livers were homogenized by motorized tissue grinder at medium setting with 15 strokes in homogenization buffer (5 mM $CaCl_2$, 3 mM $Mg(Ac)_2$, 10 mM Tris pH 7.8, 16.7 μM PMSF, 166.7 μM β-mercaptoethanol, 320 mM sucrose, 100 μM EDTA, 0.1% NP40). Samples were passed through 100 μM nylon mesh filters. Debris was removed by centrifugation for 1 min at 100 RCF at 4 °C. One volume of 50% iodixanol solution (5 mM $CaCl_2$, 3 mM $Mg(Ac)_2$, 10 mM Tris pH 7.8, 16.7 μM PMSF, 166.7 μM β-mercaptoethanol, 50% iodixano) was added to the supernatant and mixed by gentle pipetting to get a 25% solution. A 29% iodixanol solution (as before plus 160

mM sucrose) was layered underneath, and a 35% iodixanol solution (plus sucrose) was layered underneath the 29% solution. Samples were centrifuged for 20 min at 3,000 RCF at 4 ◦C with the brake off in a swinging bucket centrifuge. The nuclei band was aspirated, placed into a fresh tube and quantified using Trypan blue staining and a manual cell counter. About 50,000 nuclei were washed in ATAC-RSB buffer (10 mM Tris-HCl pH 7.4, 10 mM NaCl, 3 mM $MgCl_2$, 0.1% Tween-20), centrifuged for 10 min at 500 RCF at 4 ◦C, resuspended in Omni-ATAC Reaction Mix and proceeded to the Optimized Transposition Reaction. Illumina Nextera transposase was used for the transposition reaction [106] [107]. The reaction was cleaned up using the Zymo DNA Clean and Concentrator kit. The transposed DNA was pre-amplified using Nextera indexed primers for 5 cycles of PCR. Additional cycles of PCR were determined by qPCR using 5 µl of partially-amplified library. The resulting library was cleaned with AMPure XP beads and quantified by qPCR with Kapa Sybr Fast universal for Illumina Genome Analyzer kit. The library size was determined by analysis using the Bioanalyzer 2100 DNA High Sensitivity Chip. The library sequenced on the Illumina NovaSeq 6000 using 150 cycles and paired-end dual index read chemistry. The version of NovaSeq control software was NVCS 1.6.0 with real-time analysis software, RTA 3.4.4. Post-processing of the run to generate the FASTQ files was performed at the Institute for Genomics and Bioinformatics (UCI IGB).

ATAC-seq reads were aligned and processed following the ENCODE pipeline (https://www.encodeproject.org/atac-seq/) for paired-end sequencing reads. Reads were aligned to the mouse genome (mm9) using BowTie2 with the options of '-k 4 -X

2000'. Only properly paired reads were retained for analysis. The Picard tool (http://broadinstitute.github.io/picard/) was used to mark and remove duplicates. All samples were randomly down-sampled to 56,000,000 reads to exclude library-size effects. Read coordinates were then transformed into the 'BEDPE' format and fed to MACS2 for peak-calling. The *P*-value cutoff for MACS2 was 0.001. Peaks which overlapped with any ENCODE mm9 'blacklist' regions were excluded. The reads density in 'bedGraph' format was generated by MACS2, and then transformed to bigWig using the 'bedGraphToBigWig' tool in the UCSC binary utility directory (http://hgdownload.soe.ucsc.edu/admin/exe/). Transcription factor (TF) footprint detection was conducted on 2 biological replicates using an HMM-based software 'rgt-hint' that is able to distinguish members of the same TF family [35] with the option of '--atac-seq'. The binding difference was determined by the 'differential' module in 'rgt-hint'.

Metabolomics

Sample preparation was carried out on four biological replicates at Metabolon Inc, in a manner similar to a previous study [108]. Briefly, individual samples were subjected to methanol extraction then split into aliquots for analysis by ultrahigh performance liquid chromatography/mass spectrometry (UHPLC/MS). The global biochemical profiling analysis comprised of four unique arms consisting of reverse phase chromatography positive ionization methods optimized for hydrophilic compounds (LC/MS Pos Polar) and hydrophobic compounds (LC/MS Pos Lipid), reverse-phase chromatography with negative ionization conditions (LC/MS Neg) and a HILIC chromatography method

coupled to negative (LC/MS Polar). All methods alternated between full-scan MS and data-dependent MS^n scans. The scan range varied slightly between methods but generally covered 70–1000 *m*/*z*. Metabolites were identified by automated comparison of the ion features in the experimental samples to a reference library of chemical standard entries that included retention time, molecular weight (m/z), preferred adducts, and in-source fragments as well as associated MS spectra and curated by visual inspection for quality control using software developed at Metabolon. Identification of known chemical entities was based on comparison to metabolomic library entries of purified standards [109].

General metabolite chemical classification (lipid, carbohydrate, etc.) and sub-pathways (fatty acid synthesis, polyunsaturated fatty acid, etc.) were determined by a combination of literature evidence and cross-reference to Metabolon's internal database. Statistical analyses, including principal component analysis (PCA) and ANOVA, were carried out with MetaboAnalyst 3.0 [33] using pre-normalized peak area-under-the-curve values for each metabolite, which were then log-transformed and auto-scaled. At each ZT, ANOVA with Fisher's LSD (FDR < 0.1) determined metabolites altered in KO (WT vs KO, $P < 0.05$) and restored in liver-RE (KO vs liver-RE, $P < 0.05$; WT vs liver-RE, not significant). Outliers were removed using the Grubbs' test (ESD method). Two types of statistical analyses were performed: (1) significance tests, and (2) classification analysis. Standard statistical analyses were performed in ArrayStudio on log‑transformed data. For analyses not standard in ArrayStudio, the R program (http://cran.r‑project.org/) was used. Following log transformation and

imputation of missing values, if any, with the minimum observed value for each compound, Welch's two sample *t*-test was used as a significance test to identify biochemicals that differed significantly ($P < 0.05$) between experimental groups. An estimate of the false discovery rate (q-value) was calculated to take into account the multiple comparisons that normally occur in metabolomic-based studies. Classification analyses used included principal components analysis (PCA), hierarchical clustering, and random forest. For the scaled intensity graphics, each biochemical in original scale (raw area count) was re-scaled to set the median across all animals and time points equal to 1.

Integrated pathway and enzyme-metabolite Pair analysis

Pathway analysis integrating gene and metabolite enrichment was performed using the Integrated Molecular Pathway Level Analysis (IMPaLA) tool [110]. This analysis returned a joint enrichment *P*-value considering both genes and metabolites. Pathways were considered significantly coherent if enriched with ≥4 genes and ≥2 metabolites, $P < 0.001$.

Metabolite Correlations

For the correlation analysis, xenobiotic and partially characterized metabolites were removed from further analysis. Correlations were estimated using Pearson's correlation coefficient. Significant correlations $p< 0.01$ were selected after a FDR (Benjamini Hochberg) correction. Distance maps were calculated by subtracting the condition wise

correlation coefficients (KO, RE) from the control (WT). Overall distance was estimated as the 1-norm of the distance map.

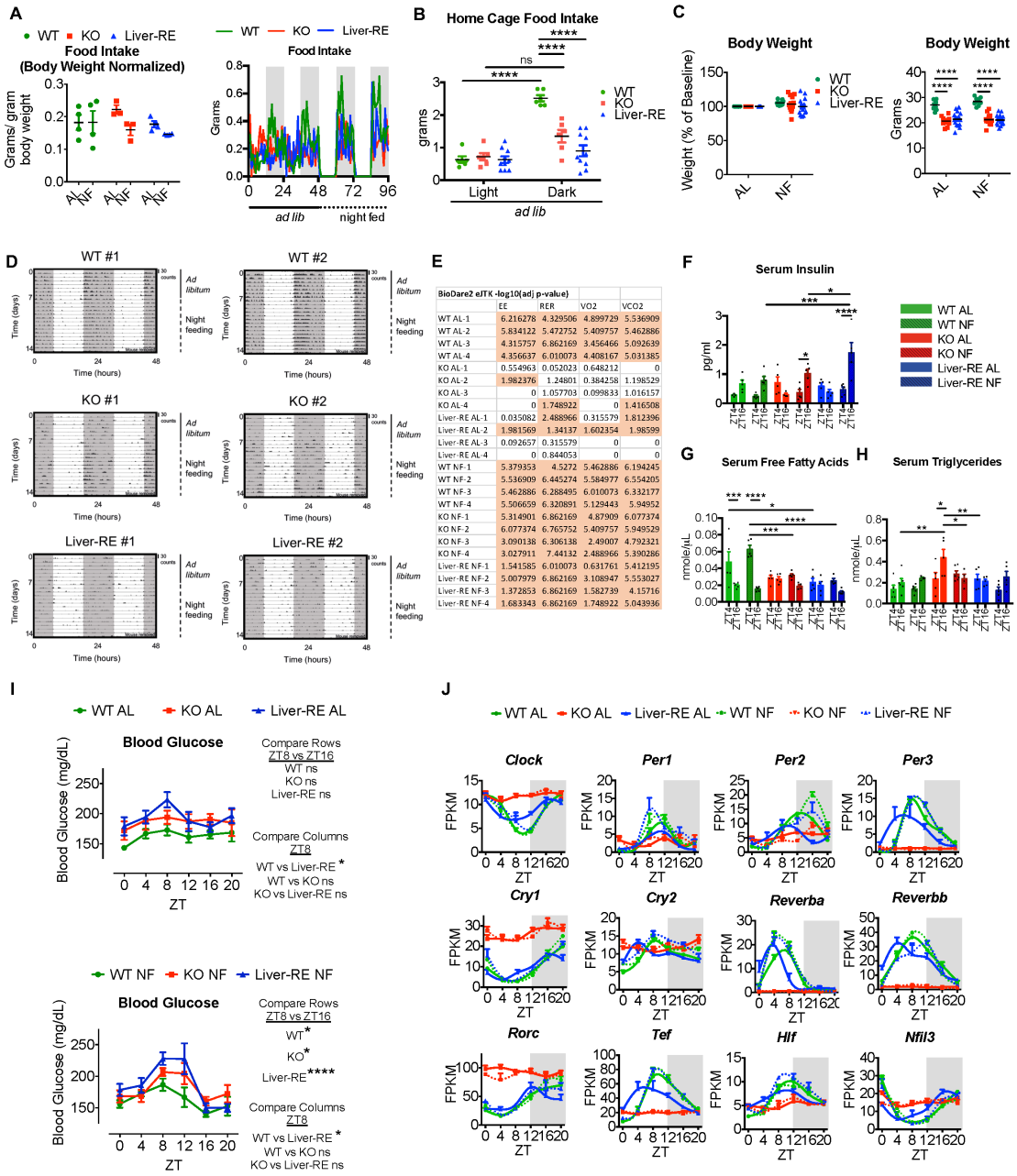

Figure S1. Metabolic characterization under ad libitum (AL) and nighttime feeding (NF). (**A**) Left - total daily food intake from metabolic cages normalized by body weight. (mean ± SEM, n= 3-4 per group; Two-way ANOVA with Bonferroni's post hoc test; no significant differences); Right – raw food intake over the diurnal cycle; AL – ad libitum,

NF – night feeding. (**B**) Food intake measured from the home cage; (mean ± SEM, n = 6–10 per group; Two-way ANOVA with Bonferroni's post hoc tests; ****, P < 0.0001; *). (**C**) Left - change in body weight from AL to NF conditions; Right – raw body weight measurements from the home cage taken immediately prior to and after NF; (mean ± SEM, n = 8–15 per group; Two-way ANOVA with Bonferroni's post hoc test; ****, P < 0.0001). (**D**) Actograms of ambulatory locomotor activity measured in home cages under AL and NF. Data scaled to 30 counts as shown by the vertical bar. Representative plots from 2 mice per genotype. (**E**) BioDare2 eJTK_CYCLE –LOG10 (P-value) for each metabolic parameter of each mouse; (n = 4; Shaded cells highlight significant oscillations; P < 0.01). (**F**) Measurements of serum insulin in each genotype under AL or NF at ZT4 and ZT16; (mean ± SEM, n=4-5; Two-way ANOVA with Bonferroni's post hoc tests; *, P <0.05; **, P <0.01; ***, P <0.001; ****, P < 0.0001). (**G**) Measurements of serum free fatty acids (FFAs) in each genotype under AL or NF at ZT4 and ZT16; (mean ± SEM, n=4-5; Two-way ANOVA with Bonferroni's post hoc tests; *, P <0.05; **, P <0.01; ***, P <0.001; ****, P < 0.0001). (**H**) Measurements of serum triglycerides in each genotype under AL or NF at ZT4 and ZT16; (mean ± SEM, n=4-5; Two-way ANOVA with Bonferroni's post hoc tests; *, P <0.05; **, P <0.01). (**I**) Blood glucose under AL (top) and NF (bottom); (mean ± SEM, n=3-12 per time point, per group; Two-way ANOVA with Tukey's post hoc tests; *, P <0.05; ****, P <0.0001). (**J**) Gene expression of clock genes from RNA-sequencing (mean ± SEM, n=3 per time point, per group).

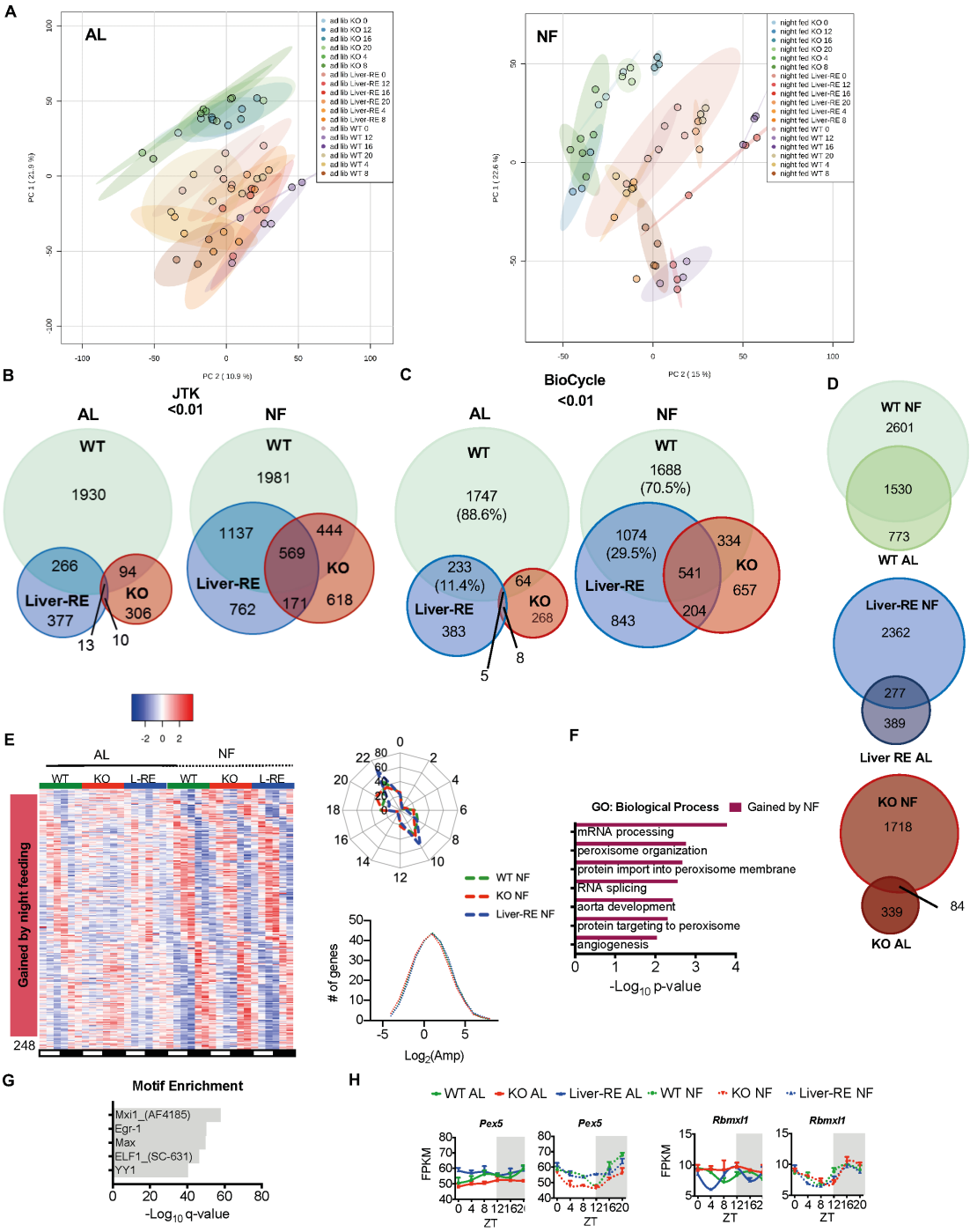

Figure S2. Liver diurnal transcriptome analysis of WT, KO and L-RE under AL and NF. (**A**) Principal component analysis (PCA) of transcriptome profiles for each ZT of each genotype under ad libitum (AL) feeding and night feeding (NF) (n=3). (**B**) Venn diagrams showing the overlap of oscillating genes under AL and NF for each genotype, as detected

by JTK_CYCLE, $P < 0.01$. (**C**) Same as (**B**) but determined by BIO_CYCLE, $P < 0.01$. (**D**) Venn diagrams showing the effect of NF on transcript oscillations within each genotype (JTK_CYCLE, $P < 0.01$). (**E**) Features of the 'gained by NF' oscillating gene class (i.e. oscillating in all NF groups but in none of the AL groups). Left - phase-sorted heatmap. Right - polar histogram of peak phases (top) and amplitude distribution (bottom, One-way ANOVA with Newman-Keuls post hoc tests; no significant differences). (**F**) Pathway enrichment for the 'gained by NF' gene class. (**G**) Motif enrichment for the 'gained by NF gene class. (**H**) Examples genes from RNA-sequencing for the 'gained by NF' gene class (mean ± SEM, n=3 per time point, per group).

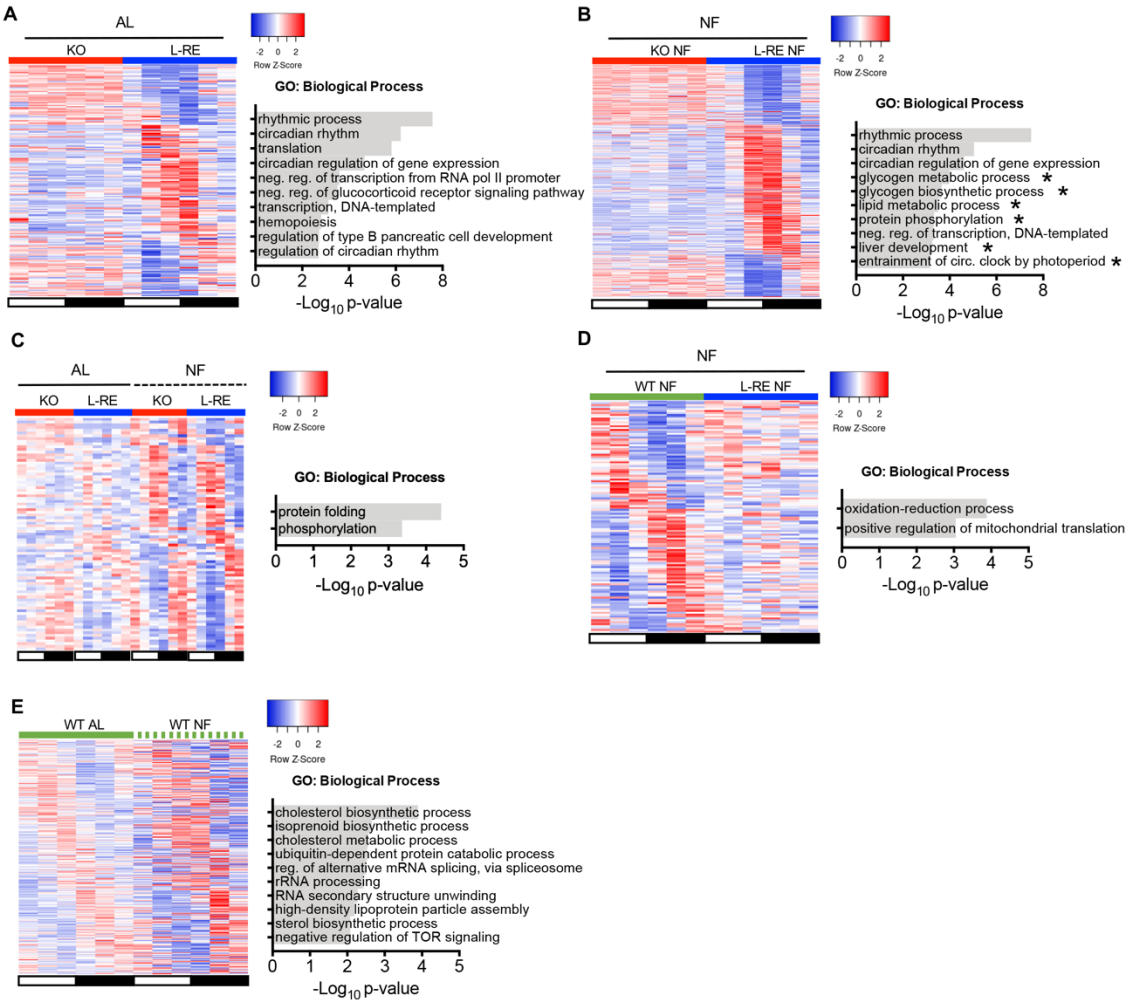

Figure S3. Differential rhythmicity analysis of the liver diurnal transcriptome. (**A-D**) Limorhyde differential rhythmicity analysis (pDR <0.01), starting from JTK_CYCLE oscillating genes (P <0.01). Left - phase sorted; right - pathway enrichment. (**A**) KO AL vs Liver-RE AL - oscillating in Liver-RE but not KO - supporting the autonomous gene class. (**B**) KO NF vs Liver-RE NF – oscillating in Liver-RE but not KO - supporting the integrated gene class (* indicates unique to NF). (**C**) Genes that gain rhythmicity under NF in both KO (KO AL vs KO NF) and Liver-RE (Liver-RE AL vs Liver-RE NF), supporting the feeding driven gene class. (**D**) WT NF vs Liver-RE NF – oscillating in WT but not

Liver-RE - supporting the network-dependent gene class. (**E**) WT AL vs WT NF – oscillating under NF but not AL - supporting the gained by NF gene class.

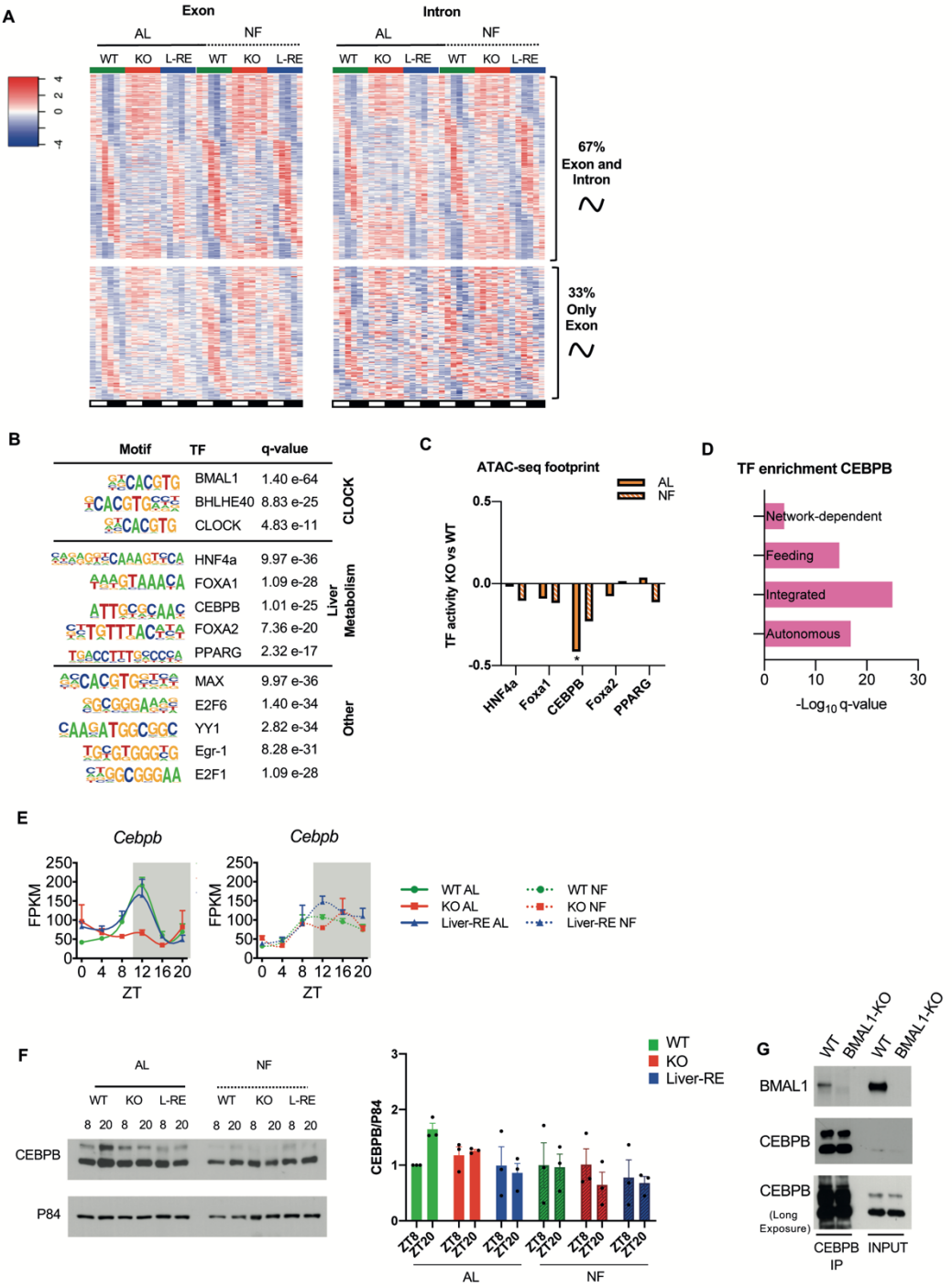

Figure S4. Identification and characterization of CEBPB as a cooperating transcription factor. (**A**) Phase-sorted heatmap of RNA-seq read coverage in exons and introns separately for Integrated genes (non-autonomous, gain oscillation in liver-RE with

NF but not KO with NF). Percentages indicate total integrated genes. (**B**) Transcription factor (TF) motif analysis of integrated genes, with motifs/TFs separate by function. (**C**) Footprint of TF binding in regions of accessible chromatin, which reflect TF activity. (n=2 per group; unpaired t-test,

*P < 0.05, Bmal1-KO vs WT). (**D**) TF motif analysis enrichment of CEBPB binding according to gene class. (**E**) Cebpb gene expression over a 24-hour cycle in each genotype under ad libitum (AL) or night feeding (NF) (mean ± SEM, n=3 per time point, per group). (**F**) Western blot analysis of CEBPB at ZT8 and ZT20 from liver whole cell extracts. Representative blots from three independent experiments are shown (left). Densitometry analysis (right, mean ± SEM, n=3 per time point, per group). (**G**) Co-immunoprecipitation (Co-IP) experiment from liver chromatin extracts using anti-CEBPB antibody at the indicated zeitgeber time (ZT8) (representative blot, n=2).

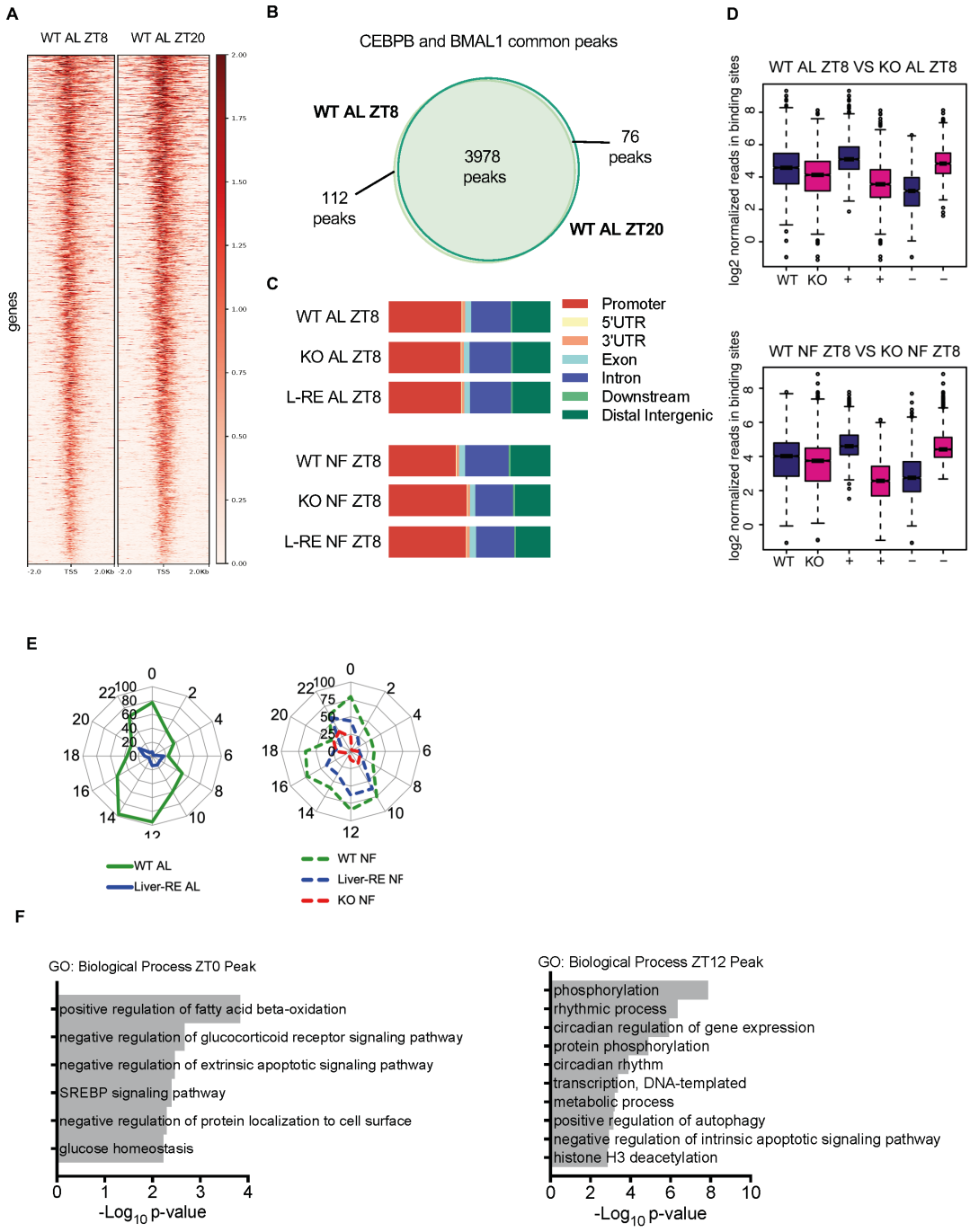

Figure S5. Characterization of CEBPB and BMAL1 DNA bound regions. (**A**) Heatmap of CEBPB ChIP-seq binding profiles for binding sites bound by both CEBPB and BMAL1 in WT ad libitum (AL) mice at zeitgeber time (ZT8 and ZT20; n=2 per time point). (**B**) Venn diagram of CEBPB and BMAL1 common binding sites identified at ZT8 and

ZT20 in livers of WT ad libitum (AL) mice. (**C**) CEBPB ChIP percent distribution over the indicated genomic regions for binding sites bound by both CEBPB and BMAL1 at ZT8 in each genotype under ad libitum (AL) or night feeding (NF). (**D**) Boxplot of distribution of reads at CEBPB- BMAL1 common binding sites over all differentially bound sites between WT AL and KO AL at ZT8. WT AL samples display overall higher mean read concentration compared to KO samples. '+' indicates sites with higher enrichment in WT samples. '–' indicates sites with higher enrichment in KO samples (DiffBind, $P < 0.05$; two-sided Wilcoxon Mann-Whitney test; n=2 per group). (**E**) Polar histogram plots of the peak phase of oscillating target genes with CEBPB and BMAL1 overlapping peaks (673 genes). (**F**) Gene ontology (GO) enrichment analysis of biological processes of oscillating target genes with CEBPB and BMAL1 overlapping peaks, grouped by phase of circadian expression.

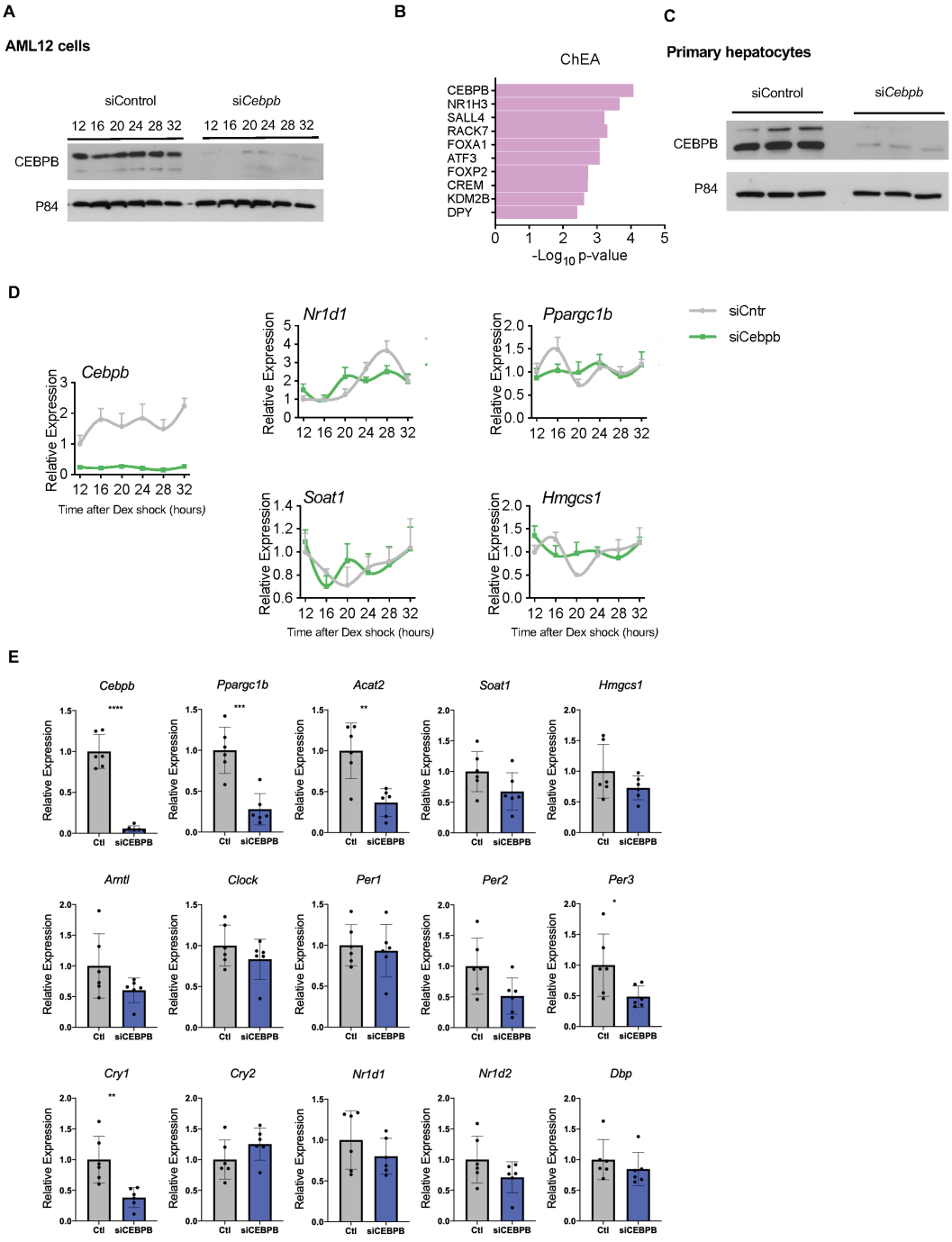

Figure S6. Knock-down of Cebpb in vitro. (**A**) Western blot analysis of CEBPB and P84 at six circadian time-points from dexamethasone (Dex) synchronized control (siControl) and Cebpb knockdown (siCebpb) AML12 cells. (**B**) ChIP Enrichment Analysis (ChEA) of the 358 genes not displaying time-dependent changes in siCebpb AML12 cells. (**C**)

Western blot analysis of CEBPB and P84 from control (siControl) and Cebpb knockdown (siCebpb) primary hepatocytes. Cells were collected 72 hours post-transfection. (**D**) Circadian expression of example genes in siControl (siCnt) and siCebpb primary hepatocytes (mean ± SEM, n=4 per time point, per group). (**E**) Gene expression analysis of metabolic and circadian genes from unsynchronised AML12 cells treated with control or siRNA targeted against *Cebpb*. Control and CEBPB siRNA concentrations of 5nM,10nM and 20nM were pooled for analysis as knockdown was similar between all concentrations. n=6 for each condition. Two-tailed unpaired t test, * $p<0.05$, ** $p<0.01$, ***$p<0.001$, **** $p<0.0001$.

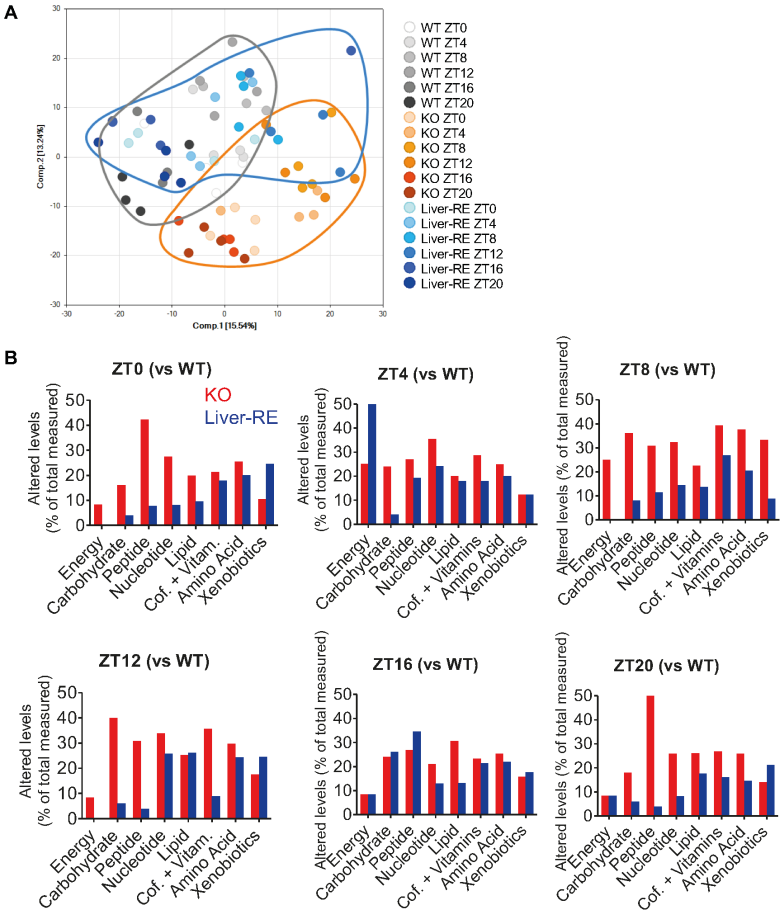

Figure S7. Global metabolite profiling under night feeding. (**A**) Principal component analysis (PCA) of metabolite profiles under night feeding (NF); (n=4 per group, per time point). (**B**) One-way ANOVA comparisons between genotype of each metabolite at each ZT; (n=4 per group, per time point; $P < 0.05$).

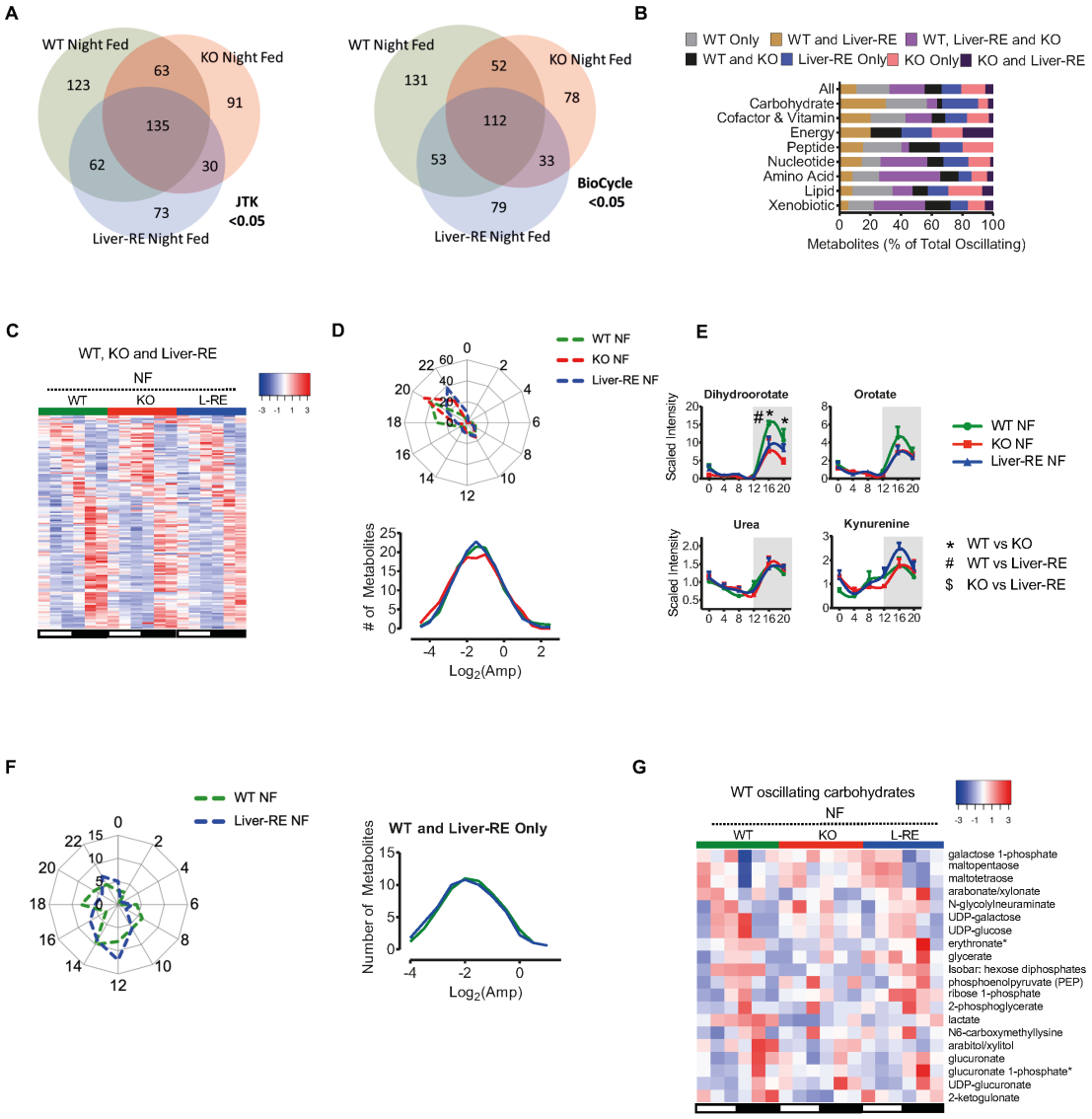

Figure S8. Metabolomics analysis over circadian time under night feeding. (**A**) Venn diagram showing overlap of oscillating metabolites by JTK_CYCLE (left) and BIO_CYCLE (right) with night feeding (NF); (n=4 per group, per time point; P<0.01). (**B**) Overlap as in (**A**), broken down into chemical classes. (**C**) Phase-sorted heatmap of metabolites oscillating in WT, KO and Liver-RE under NF. (**D**) Polar histogram of peak phase and amplitude distribution of metabolites oscillating in WT, KO and Liver-RE under

NF. (**E**) Examples of metabolites; (mean ± SEM, n=4 per group, per time point; two-way ANOVA with Bonferroni post hoc tests; $P < 0.05$; *, WT vs KO; #, WT vs liver-RE). (**F**) Polar histogram of peak phase and amplitude distribution of metabolites oscillating in WT and liver-RE only under NF. (**G**) Phase-sorted heatmap of all oscillating carbohydrates in WT.

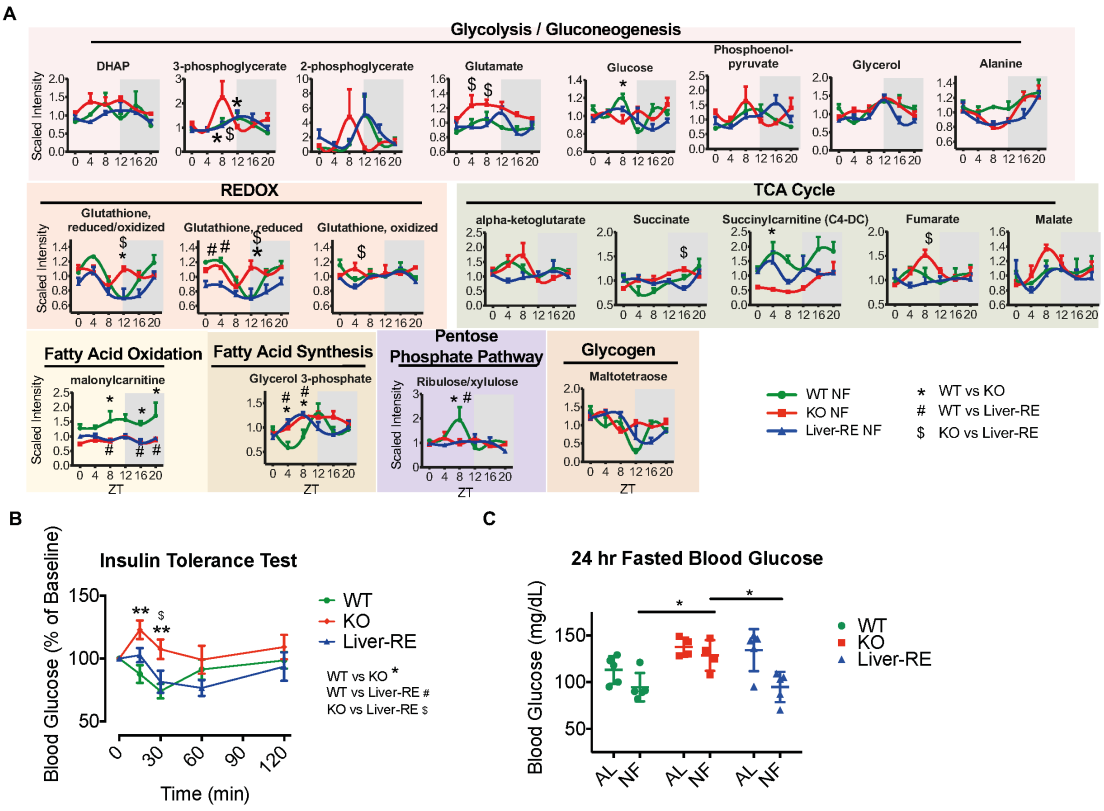

Figure S9. Examples of metabolites in liver metabolic pathways and insulin tolerance test. (**A**) Key metabolites related to Figure 4. (mean ± SEM, n=4 per group, per time point; Two-way ANOVA with Bonferroni post hoc tests; $P < 0.05$; *, WT vs KO; #, WT vs liver-RE; $, KO vs liver-RE). (**B**) Insulin tolerance test under ad libitum feeding (AL). Mice were fasted from ZT0 to ZT4, and then injected IP (0.3U/kg insulin). (mean ± SEM, n= 5-7 per group; Two-way ANOVA with Tukey's post hoc tests; *P <0.05, **P <0.01). (**C**) Mice were fasted for 24 hr from ZT0 to ZT24/0 and blood glucose was measured. (mean ± SEM, n= 4-5 per group; Two-way ANOVA with Bonferroni post hoc tests; *P <0.05).

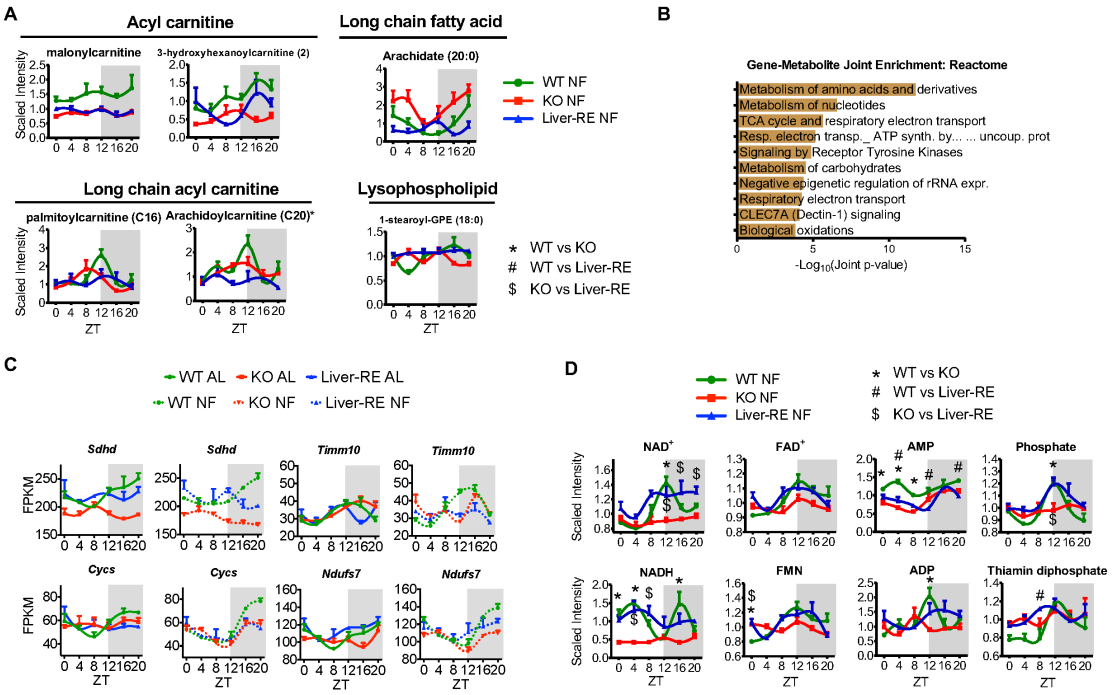

Figure S10. Network-dependent genes and metabolites. (**A**) Examples of WT- only oscillating and other key lipid metabolites that participate in fatty acid metabolism (mean ± SEM, n=4 per group, per time point). (**B**) IMPaLA joint gene-metabolite enrichment analysis of Reactome pathways of WT-only oscillating genes and metabolites. (**C**) Example of related network-dependent genes (mean ± SEM, n=3 per group, per time point). (**D**) Metabolites that oscillated exclusively in WT related to mitochondrial function. (mean ± SEM, n=4 per group, per time point; Two-way ANOVA with Bonferroni post hoc tests; $P < 0.05$; *, WT vs KO; #, WT vs liver-RE; $, KO vs liver-RE).

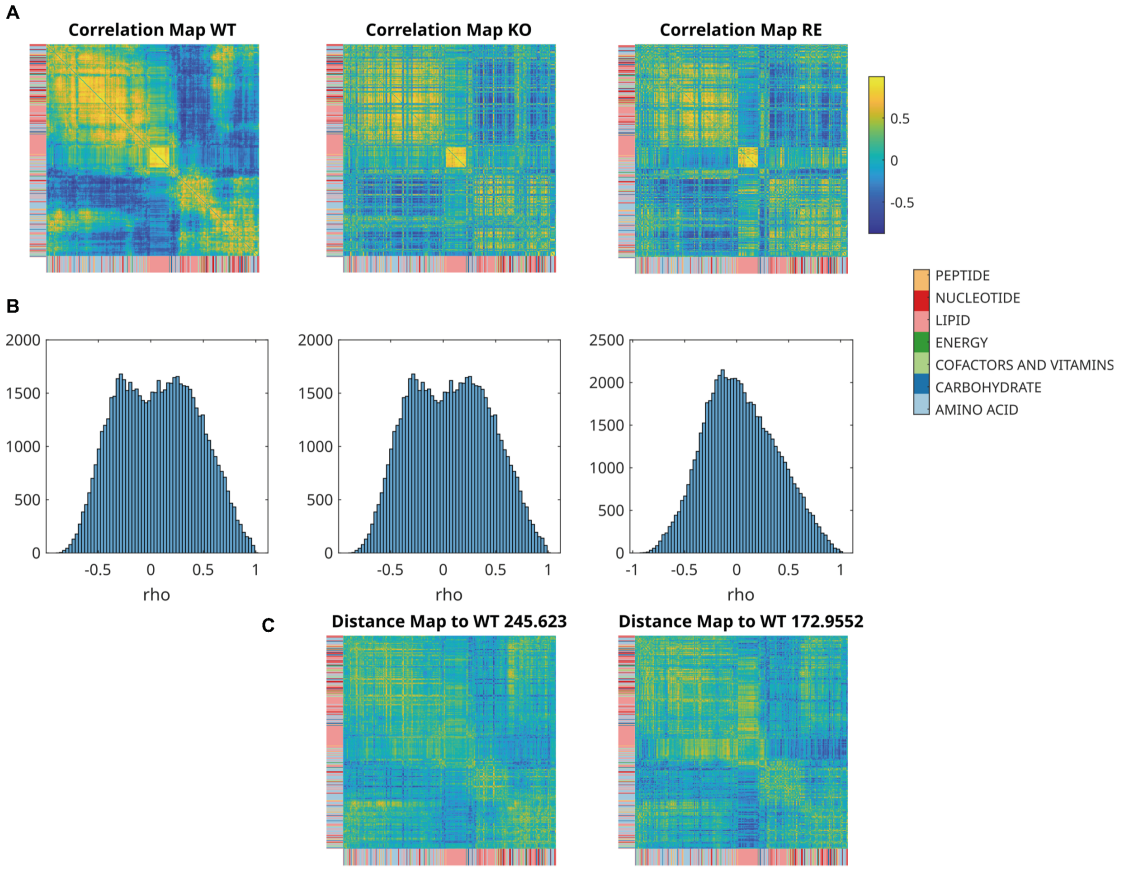

Figure S11. Metabolite correlations. (**A**) Metabolite pairwise correlation heatmaps encompassing all detected metabolites, according to genotype. (**B**) Histograms showing distributions of corresponding Rho-values. (**C**) Distance maps show Δ Rho (ρ) values comparing KO and RE correlation coefficients to the WT. Overall distance estimates refer to the 1-norm of the distance maps.

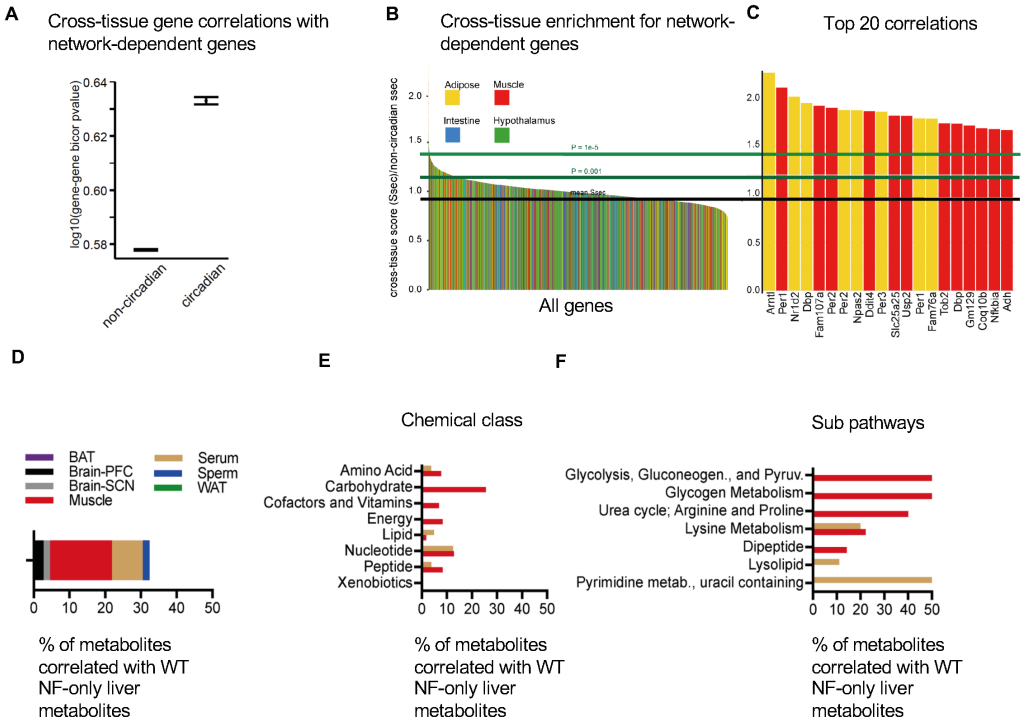

Figure S12. Unrestored transcriptional and metabolic rhythms are correlated with clock and metabolic function in extra-hepatic tissues. (**A**) Enrichment of network-dependent liver genes with circadian genes in other tissues (n=3 per group). (**B**) Cross-tissue correlations between network-dependent circadian genes in liver and all genes in the indicated extra-hepatic tissues. (**C**) Top 20 genes correlated with network-dependent genes in liver. (**D**) Cross-tissue metabolite correlation analysis with metabolites oscillating in WT liver only, using dataset from (Dyar et al., 2018) and displayed with respect to the percentage of total detected metabolites in each region (n=4 per group). Cross-tissue metabolite correlations in muscle and serum with WT only liver metabolites are displayed with respect to chemical classes (**E**) and sub-pathways (**F**).

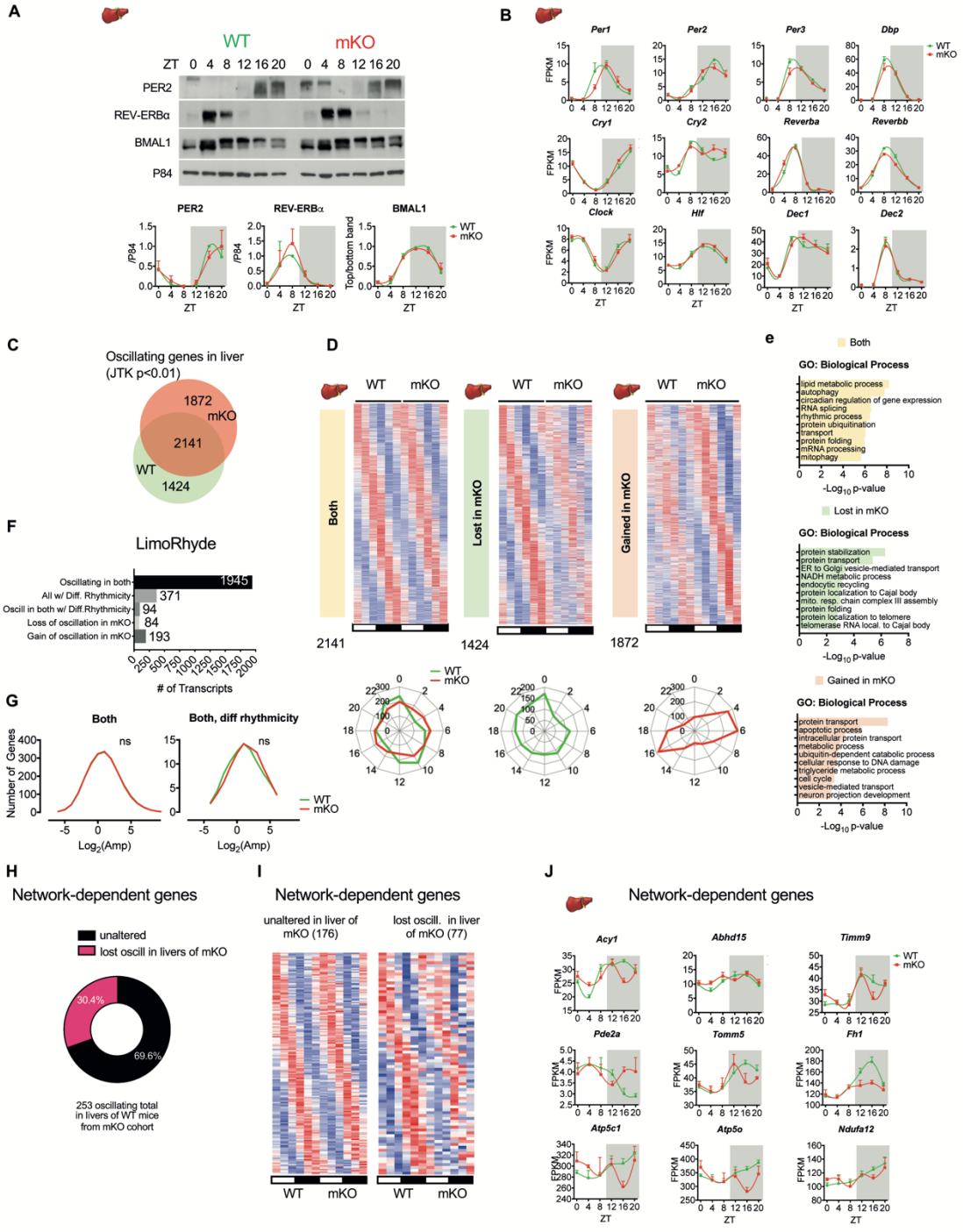

Figure S13. Characterization of liver circadian rhythms in BMAL1 muscle-specific knockout mice (mKO). (**A**) Western blotting of clock proteins PER2, REV- ERBα and BMAL1 in livers of WT and mKO mice, p84 used as loading control. (Representative blot,

densitometry from n=4 mice per time point per genotype- normalized to P84, the PER2 expression at ZT16 within each blot, and REV-ERBα at ZT8. BMAL1 densitometry is displayed as ratio between higher and lower molecular weight band. Data displayed as mean ± SEM.) (**B**) Analysis of core clock gene expression in livers from WT and mKO mice (mean ± SEM, n=3 per group, per time point). (**C**) Oscillating genes in livers from WT and mKO by JTK analysis, using $P<0.01$ to define rhythmicity (n=3 per group, per time point). (**D**) Phase-aligned heatmaps of genes oscillating in both genotypes, versus those lost in mKO or gained in mKO as defined by JTK, as well as phase plots for each subset. (**E**) Gene- ontology analysis of oscillatory gene classes defined by JTK. (**F**) Bar chart showing subsets of genes defined after LimoRhyde analysis for differential rhythmicity (n=3 per group, per time point; pDR <0.01). (**G**) Amplitude histograms for genes defined as oscillating in both conditions with unaltered or altered rhythmicity by LimoRhyde. (**H**) Network dependent genes (Fig. 2F) were overlapped with oscillating genes from JTK dataset from WT livers (of mKO cohort) (253 genes total). Effect of muscle-specific knockout on oscillation of these network-dependent genes is shown, with accompanying heatmaps (**I**) and examples of network-dependent genes lost in mKO (mean ± SEM, n=3 per group, per time point) (**J**).

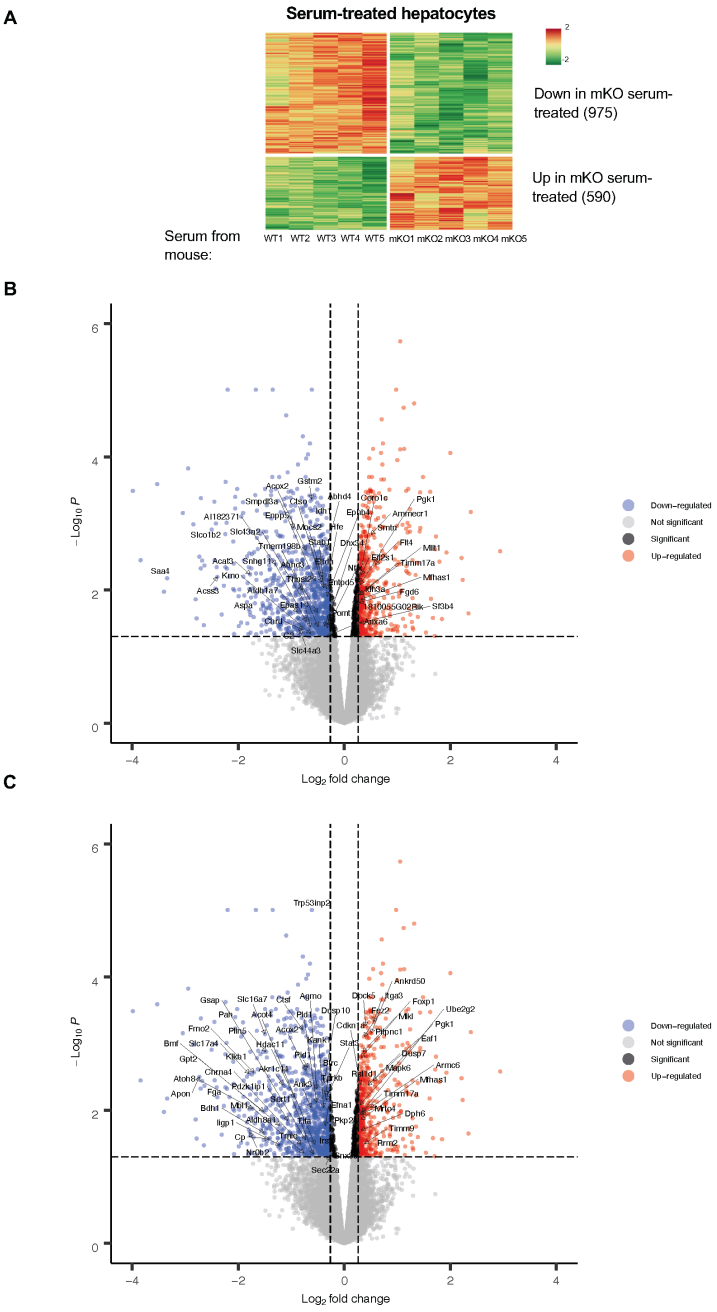

Figure S14. Analysis of differential gene expression in hepatocytes treated with serum from WT and BMAL1 muscle-specific knockout mice. (**A**) Heatmap showing clustering of genes in hepatocytes treated with serum from either WT or BMAL1 muscle- specific knockout mice (mKO). Effect of serum treatment from individual WT or BMAL1 mice is

shown (hepatocytes were treated with n=5 individual serum samples as listed). (**B**) Volcano plot with genes identified as altered in mKO livers labelled with arrows (FDR <0.05). (**C**) Volcano plot with genes also identified as network-dependent in liver labeled with arrows (FDR <0.05).

Data S1. (separate file)

JTK cycle Analysis of RNA-seq data from WT, L-RE, KO AL and NF

Data S2. (separate file)

LimoRhyde Differential Rhythmicity Analysis related to Supplementary Table 1

Data S3. (separate file)

ATAC-seq Footprint Differential Analysis of WT, L-RE, KO AL and NF at ZT8

Data S4. (separate file)

List of genomic regions co-bound by BMAL1 and CEBPB in WT AL at ZT8 and ZT20 and in WT NF, L-RE AL and NF, KO AL and NF at ZT8

Data S5. (separate file)

RNA-seq Differential Analysis of siControl and siCebpb AML12 cells 12 and 24 hours post dexamethasone synchronization

Data S6. (separate file)

JTK cycle Analysis of Metabolome Data from WT, L-RE, KO NF

Data S7. (separate file)

QENIE analysis of Network-dependent genes

Data S8. (separate file)

JTK cycle and LimoRhyde Differential Rhythmicity Analysis of RNA-seq data from Livers of WT and muscle specific BMAL-KO mice (mKO)

Data S9. (separate file)

RNA-seq Differential Analysis of primary hepatocytes treated with serum from WT and mKO mice for 24 hours